RESEARCH PAPER

Nesfatin-1 Ameliorated Cognitive Functions In L-Methionine-Induced Vascular Cognitive Impairment and Dementia By Restoring Brain Mitochondrial Activity

Gaganjit Kaur[1,2], Sushma Devi[1], Manish Shukla[3], Manish Kumar[4*]

[1]Chitkara College of Pharmacy, Chitkara University, Rajpura, Punjab 140417

[2]Maharaja Agrasen School of Pharmacy, Maharaja Agrasen University, Baddi, Solan, Himachal Pradesh, India 174103

[3]Department of Neurosurgery, Penn State College of Medicine, Penn State Health Milton S. Hershey Medical Center, PA, 17033, USA

[4*]M.M. College of Pharmacy, Maharishi Markandeshwar Deemed-to-be-University, Mullana, Ambala, Haryana 133207. Corresponding Author: Dr. Manish Kumar (PhD, M. Pharm), Associate Professor, Department of Pharmacology. Phone No. +91-9050757400, +91-9896980896.

Email: mkpharmacology@gmail.com, manish_kumar@mmumullana.org

Running Title: Nesfatin-1 attenuated L-methionine neurotoxicity

Abstract

L-Methionine-induced hyperhomocysteinemia (HHcy) causes vascular anomalies such as endothelial dysfunction and mitochondrial impairment that triggers vascular cognitive impairment and dementia (VCID). Nesgatin-1 is an anorexigenic peptide that might protect the brain against neurotoxicity of L-methionine (LM). The present work investigated the mitochondria-targeted neuroprotective potential of nesfatin-1 in an L-methionine–induced rat model of HHcy-associated VCID. LM (1.7 g/kg/day) was administered for 8 weeks in Wistar rats (adult males) to induced VCID. Nesfatin-1 (0.3, 1, and 3 μg/kg) was administered intracerebroventricularly (ICV) for 2 weeks. We observed that LM-induced HHcy defunctionalized mitochondrial enzyme activity, lowered ATP levels, and triggered oxidative stress and inflammation (tumor necrosis factor-α, interleukin-1β) in the brain of rats. LM induced a rise in vascular injury markers (matrix metalloproteinase-9) and chemokines (monocyte chemoattractant protein-1) in the brain. Nesfatin-1 ICV treatment attenuated L-Met–induced brain oxidative stress, inflammation, vascular injury, and chemokine levels. The activity of acetylcholinesterase and glutamate levels were decreased and GABA was increased significantly by nesfatin-1. Nesfatin-1 significantly improved brain mitochondrial respiratory chain activity (complex I, II, IV, and V), endothelial nitric oxide synthase (eNOS) activity, PGC-1α, and attenuated apoptotic factors (caspase-3/-9 and cytochrome-*c*). Nesfatin-1 significantly improved spatial learning and memory and working memory in rats against LM in HHcy-induced VCID model. Collectively, these findings provide compelling evidence that nesfatin-1 confers robust neuroprotection against HHcy-induced VCID. Nesfatin-1 emerges as a promising therapeutic candidate for targeting mitochondrial dysfunction in VCID.

Keywords Vascular dementia, L-methionine, Nesfatin-1, Matrix metalloproteinase-9, Mitochondria, Apoptosis

How to cite this article: Kaur G, Devi S, Shukla M, Kumar M. Nesfatin-1 Ameliorated Cognitive Functions In L-Methionine-Induced Vascular Cognitive Impairment and Dementia By Restoring Brain Mitochondrial Activity. Int J Drug Deliv Technol. 2026;16(18s): 153-173. DOI: 10.25258/ijddt.16.18s.16

1. Introduction

Vascular contributions to cognitive impairment and dementia (VCID) encompass a spectrum of cognitive disorders driven by cerebrovascular pathology, ranging from mild deficits to frank dementia (Silva et al., 2022). Characterized by conditions such as small vessel disease, cerebral amyloid angiopathy, and strategic infarcts, VCID results from compromised cerebral blood flow and neurovascular unit dysfunction, leading to white matter damage and neuronal injury (Jiménez-Ruiz et al., 2024). While vascular dementia (VaD) is recognized as the second most common cause of cognitive impairment after Alzheimer's disease (AD), neuropathological studies reveal that pure vascular dementia is relatively rare; instead, the majority of cases exhibit mixed pathology, with cerebrovascular disease commonly

coexisting with and exacerbating AD pathology Cerebral amyloid angiopathy (CAA) and small vessel diseases (SVD) are common in neocortical areas and basal ganglia, respectively (Gorelick et al., 2016). Vascular dementia (VaD) is the second most prevalent basis of dementia after Alzheimer's disease (AD) due to a recent decrease in cardiovascular risk factors. The global burden of dementia is 5.7×10^6 (2021), and 5-10% of dementia cases include VaD. At present, there is no FDA-approved drug treatment specific for VaD, however, drugs for AD and the underlying diseases, such as hypertension, obesity, diabetes, etc., are used for the treatment of vascular dementia with limited success (Smith et al., 2025) (Khodir et al., 2022).

Among the myriad modifiable vascular risk factors, hyperhomocysteinemia (HHcy) has garnered considerable attention for its strong association with cognitive decline and cerebral microvascular degeneration. Elevated homocysteine (Hcy) disrupts endothelial nitric oxide (NO) signaling, promotes excitotoxicity, enhances mitochondrial permeability transition, and increases neuroinflammatory and apoptotic cascades, ultimately impairing neuronal survival and synaptic plasticity (Moosavi et al., 2014; Alachkar et al., 2022). Experimental models of VCID induced by chronic L-methionine (L-met) administration reproducibly mimic the biochemical, vascular, and neurobehavioral alterations (Hemanth Kumar et al., 2017) associated with HHcy in humans, thereby providing a robust platform to investigate mitochondrial and endothelial-based neuroprotective strategies.

Mitochondrial dysfunction is a central mechanistic driver in the pathogenesis of VCID (He et al., 2024; Patai et al., 2025). Excess homocysteine (Hcy) and its metabolite homocysteic acid compromise respiratory chain complexes, impair membrane potential, adenosine triphosphate (ATPs) and calcium (Ca^{2+}) homeostasis, and promotes cytochrome-*c* release *via* opening of the mitochondrial permeability transition pore (mPTP) (Zhang et al., 2020). Hcy inhibits tricarboxylic acid (TCA) cycle *via* reduction in aconitase and the UQCRC2 (Ubiquinol-Cytochrome C Reductase Core Protein 2) component of complex III. Hcy elevates mitochondrial reactive oxygen species (ROS) leakage, impairs antioxidant mechanisms (e.g., MnSOD, Nrf2 pathway), and enhance ROS-producing enzymes, such as NADPH oxidase (Nox) and nitric oxide synthase (NOS) (Kaplan et al., 2020). HHcy can alter mtDNA, epigenetic mechanisms, and induce mitochondrial apoptotic pathways through several mechanisms, such as endoplasmic reticulum (ER) stress and excitotoxicity, that might alter mitochondrial dynamics (e.g., mitochondrial fission and fusion) (Chen et al., 2021; Škovierová et al., 2016). These events collectively impair neuronal energy metabolism and accelerate cognitive deficits. Thus, therapeutic interventions that stabilize mitochondrial bioenergetics, preserve membrane potential, reduce oxidative overload, and prevent inflammatory signaling represent a promising approach for mitigating VCID progression.

Nesfatin-1, an 82-amino acid peptide derived from nucleobindin-2 (NUCB2), has recently emerged as a pleiotropic neuroprotective factor (Zhou and Nao, 2024). Preclinical studies have demonstrated its capacity to activate pro-survival signaling pathways, including PI3K/Akt and ERK1/2, thereby preserving mitochondrial membrane potential, inhibiting cytochrome c release, and attenuating neuronal apoptosis in models of neurotoxicity (Tan et al., 2015). While these antioxidant, anti-apoptotic, and endothelial-stabilizing properties have been observed in various contexts of metabolic and ischemic brain injury (Damian-Buda, 2024), its specific mechanistic role in mitochondria-targeted neuroprotection against HHcy-induced VCID has not been explored. The present study was designed to investigate the mitochondria-targeted neuroprotective effects of nesfatin-1 in an experimental rat model of HHcy-induced VCID. Specifically, the study aimed to evaluate the effect of nesfatin-1 on cognitive performance, including spatial learning and memory, as well as to assess its impact on serum biochemical alterations induced by L-methionine (Schalla and Stengel, 2018). The L-methionine–induced hyperhomocysteinemia model is a well-established and clinically relevant paradigm that replicates hallmark features of human VCID, including oxidative stress, endothelial dysfunction, mitochondrial injury, and cognitive deficits. Through intracerebroventricular administration, this study ensures direct engagement of nesfatin-1 with central mitochondrial and vascular targets. The comprehensive study design, incorporating multiple mitochondrial biomarkers, behavioral assays, and histological evaluations, facilitates a thorough mechanistic exploration of nesfatin-1–mediated neuroprotection.

2. Material and Methods

2.1. Experimental Animals

Protocol no. SSP/IAEC/2025/014 was approved by IAEC in May 2025. Adult male Wistar rats ranging around 220 and 250 g were acquired and kept in controlled environments (22±2°C, 12-h light/dark cycle, 55–65% humidity) with unlimited access to water and a regular pellet diet. The CCSEA, New Delhi recommendations and ARRIVE criteria were followed in every procedure. Rats fasted for 12 h before to surgery as part of the pre-surgical procedures, although they were allowed to drink water *ad libitum*. Regarding the various therapy regimens provided to animal cohorts, the animal handlers and custodian were blinded. Every animal-based study was conducted from 0900 to 1500 h in a single day. 14 days before the experiment, the animals were acclimated.

2.2. Drugs treatment schedule

The rats were divided into 7 groups (n = 8): i) V+Sham group received vehicle and sham surgery, ii) LM+Sham group received L-Met and sham surgery, iii) N(3) *per se* group was given Nesfatin-1 (3 μg/kg), iv) LM+N(0.3) group was given L-Met and Nesfatin-1 (0.3 μg/kg), v) LM+N(1) group was given L-Met and Nesfatin-1 (1 μg/kg), vi) LM+N(3) group was given L-Met and Nesfatin-1 (3 μg/kg), vii) LM+P group was given L-Met and piracetam (500 mg/kg, *p.o.*). VCID was induced in rats by chronic oral administration of L-methionine (LM; 1.7 g/kg/day) for 8 weeks. This regimen reliably elevates serum Hcy and evokes cerebrovascular and cognitive deficits characteristic of VCID (Bhatia and Singh, 2021). At the start of 5th week, an ICV cannula was implanted. Nesfatin-1 (doses 0.3, 1, and 3 μg per kg body weight in 5 μl volume of aCSF) (Goebel *et al*., 2011; Dore *et al*., 2020; Shimizu *et al*., 2009; Mortazavi *et al*., 2015; Dong *et al*., 2013; Arabaci Tamer *et al*., 2022) was administered ICV for 14 days (day 43 to 56). Piracetam, standard nootropic drug, (dose 500 mg/kg) was given orally for 14 days (Chester *et al.*, 2017; Wang et al., 2020). Equal amount of vehicle was administered in the vehicle control and LM control groups. Body weight and feed/water intake was monitored each day and analyzed weekly. Locomotor activity and motor coordination of rats was evaluated on day(s) 1, 49, and 56. The Morris water maze test was performed to evaluate the long-term spatial memory of rats. Acquisition trials were performed from day 57-61 and retention trial was performed on day 62. Novel object recognition task was conducted on day 63 to assess the working memory of rats.

2.3. ICV cannula implantation in rats

The rats were anesthetized (ketamine, 80 mg/kg, *i.p.* and xylazine, 10 mg/kg, *i.p.*), the hair were removed, and an incision was given in the skin to open the skull of the rat. An analgesic (equal parts of lidocaine and bupivacaine) was used and a burr hole was created using stereotaxic apparatus (anteroposterior from bregma = −0.8 mm, mediolateral from mid-sagittal suture = ± 1.5 mm, and dorsoventral from the skull = ± 3.6 mm) (Paxinos and Watson, 1986). The intracerebroventricular (ICV) guide cannula (heparinized), was rooted 3.6 mm underneath the skull surface by using dental cement. A 28-gauge stainless steel stylet was introduced into the cannula to block the opening. For ICV injections the stylet was removed. Again, the surgical wound was applied with local anesthetic, the skin was sutured, Reflin® (cephazolin sodium, 30 mg/kg, *i.p.,* Ranbaxy) was injected. Neosporin® (GSK, Mumbai) was applied for 6 days. Meloxicam (2 mg/kg) was given orally for 3 days. To avoid dehydration, lactated Ringer's solution (5 ml) was administered subcutaneously (*s.c.*). The body temperature at 37±0.5°C was maintained using a heating pad (Kumar and Bansal, 2018).

2.4. Locomotor activity

Animal was positioned in the actophotometer (INCO, Ambala, India) for habituation (5 min) and then observed for 10 min and stated as counts per 10 min (Kumar et al., 2021; Reddy and Kulkarni, 1998).

2.5. Rotarod test

The rats were made proficient (≥ 60 s fall-off time at 9 rpm) on the apparatus. Each rat was positioned on the cylindrical shaft whose rotation was incrementally amplified (over 50 s) every 10 s from 6 rpm (1st speed) to 30 rpm (5th speed) and fall-off time (s) was observed for 5 min (Oyamada et al., 2008; Reddy and Kulkarni, 1998). The results are expressed as latency to fall-off (s).

2.6. Morris water maze test

Memory (spatial) was evaluated in three phases: acquaintance, acquisition, and retention. A circular tank pool of black color (200 cm × 60 cm, half-filled with water, 25±1°C) was separated into 4 alike quadrants

designated north (N), east (E), south (S) and west (W) (clockwise). A platform [area 11 cm^2, task difficulty ratio (search area: target ratio) of 314:1] was placed north-west (NW), 2 cm below water surface and disguised by making the water opaque with a non-toxic water color. Each rat was allowed to travel the maze for 120 s without platform. In acquisition phase, each animal received 4 consecutive trials each day with inter-trial gap (ITG) of 30 s with unaltered position of the camouflaged platform. The drop location of rat was changed each day for each trial for 5 days during acquisition trials and permitted 120 s to trace underwater dais. Mean escape latency (MEL) was noted. 24 h after last acquisition trial, memory retained was assessed in which the platform was removed and animal placed 180° from original platform location was permitted to discover the pool for 60 s. Time spent in target quadrant (TSTQ) probing for the concealed platform refers to retrieval memory (Morris, 1984, Vorhees & Williams, 2006).

2.7. Novel object recognition task

An open wooden box (80×40×60 cm^3) was positioned in a sound-attenuated area illumined by a 60W bulb. The trial consisted of habituation (P1), acquisition (P2) and retrieval phase (P3). P1 was performed for 3 successive days prior to testing and rats were allowed to explore the box area for 5 min. In P2, rats were allowed to explore the 2 indistinguishable immovable wooden objects of different shapes and color (placed 10 cm separate from walls at opposite ends) in the box for 5 min. Exploration referred to directing the snout near the item ≤ 2 cm or touching the object. After an intertrial interval (ITI) of 60 min, P3 started. In P3, rats were allowed to explore two different objects (one familiar and other novel) while counterbalancing all the combinations and location of objects to eliminate the potential bias. 20% ethanol was used to clean the objects. The time spent exploring each article in P2 and P3 was manually noted. The total exploration time for two identical objects in P2 (E1 = EA1 + EA2) and the exploration time for two different objects in P3 (E2 = EA3 + EB) was calculated. Retention of memory is given by EB – EA3. Discrimination index is calculated by DI = (EB – EA3) / (EA3 + EB) and expressed as % DI (Ennaceur and Delacour, 1988).

2.8. Blood sample preparation

The blood samples *via* retro-orbital venipuncture were collected in Eppendorf tubes and allowed at room temperature to clot for 21 min. The coagulate was separated with a glass stirrer and then centrifuged for 15 min at 3000 rpm speed in order to separate the serum. Blood lipoproteins levels were estimated as per the colorimetric kit instructions.

2.9. Preparation of brain samples

Diethyl ether anesthesia was used and animals were then decapitated (Saxena *et al.*, 2010). Whole brains were dissected out, rinsed with ice-cold isotonic saline (0.9% NaCl) while placed on ice and weighed. Potter-Elvehjam-type glass homogenizer was used to prepare mitochondria fractions of 10% w/v homogenate by using ice-cold mitochondrial separation 10 ml buffer A (225 mM mannitol, 75 mM sucrose, 1 mM EGTA, 1 mg/ml BSA, 5 mM HEPES, pH 7.4) (Khan et al., 2005; Kamboj et al., 2008; Puka-Sundvall *et al.,* 1995). 20 ml of buffer A was again added and mixture was centrifuged at 4 °C (2000 × *g*, 3 min). The supernatant was conserved. Pellet was again centrifuged (12,000 × g for 8 min) in buffer A (10 ml) using 4 tubes. The pellet was added with buffer A (10 ml) and digitonin (0.02%) to lyse the synaptosomes, and then again centrifuged (12,000 × *g* for 10 min). Buffer A was prepared lacking BSA/EGTA and mitochondrial pellet was washed and resuspended in a suitable buffer for biochemical investigations. For the measurement of Complex I, II, IV, V, mitochondrial permeability transition (MPT), and citrate synthase (CS) activity, phosphate buffer (50 mM, pH 7.4) was added to mitochondrial pellet (−20 °C temperature) that were utilized within 3 days. The previously separated homogenate was used to evaluate biomarkers of inflammation, apoptosis, eNOS, and PGC-1α. Myeloperoxidase (MPO) activity, a biomarker of inflammatory neutrophil extravasation, was assessed using mitochondrial pellet and expressed as Units/mg protein (Grisham et al., 1990). The total protein in the brain homogenate was measured by following the procedure given by Lowry et al. (1951).

2.10. Estimation of serum homocysteine levels

Dithiothreitol (1 ml) and Tris buffer (9 ml) (Solution A) was mixed. Reducing agent, dithiothreitol, freed the complexed homocysteine. The Solution A (2 ml) was added with methionine α,γ-lyase solution (1 ml). Sample (20 µl) was added with solution A (200 µl), incubated (room temperature, 5 min), added with an oxidant, and re-incubated at room temperature (5 min). Hydrogen

sulfide (H_2S) produced by methionine α,γ-lyase reacts with chromophore having absorbance at 660 nm and measured as μM homocysteine (Zhao et al., 2015).

2.11. Estimation of serum nitrite content

A copper and cadmium alloy (10% w/w) was activated using 0.5 N HCl. To the supernatant (0.1 ml) carbonate buffer (0.4 ml, pH 9) and alloy (150 mg) was added followed by incubation at room temperature (60 min). Sodium hydroxide (0.35 m) and zinc sulfate (120 mM) were added to the assay mixture and then centrifuged (4000 rpm for 10 min). Supernatant (0.1 ml) was treated with 0.5 ml of Greiss reagent (1:1 solution of 1% sulphanilamide in 3 M HCl and 0.1% *N*-1-Napthyl ethylene diamine dihydrochloride in water), incubated in dark, and absorbance noted at 548 nm. The concentration of unknown sample was calculated from the standard curve between absorbance and concentration of sodium nitrite (10-100 μM). Nitrite content is stated as μmol/mg of protein (Sastry et al., 2002).

2.12. Estimation of biomarkers of oxidative stress, inflammation, and neurotransmitters in the brain

Thiobarbituric acid reactive substances (TBARS) (Ohkawa *et al.* 1979), reduced glutathione (GSH) (Ellman, 1959), superoxide dismutase activity (Suzuki, 2000), catalase activity (Claiborne, 1985), and protein carbonyl (Yan et al., 1995; Reznick and Packer, 1994) content was evaluated. A double-beam UV-Vis spectrophotometer was used to detect the absorbance of the chromophore. Molar extinction coefficient of chromophore $1.56\times10^5\ M^{-1}cm^{-1}$ at 532 nm was used for calculation of total TBARS content. The quantity of glutathione (μmol GSH/mg protein) was measured using molar extinction coefficient (ε) $1.36\times10^4\ M^{-1}cm^{-1}$ of the chromophore at 412 nm. SOD activity is expressed in units of SOD per mg of protein. Catalase (CAT) enzymatic activity (μmol H_2O_2 decomposed/min/mg protein) was determined utilizing molar extinction coefficient (ε = 43.6 $M^{-1}cm^{-1}$ at 240 nm). To determine protein carbonyls, the separated protein was suspended in 1 mL of denaturing buffer and absorbance noted at λ_{max} = 370 nm spectrophotometrically. Protein carbonylation was quantified using ε = 22,000 /M/cm (Hissin and Hilf, 1976). Double antibody sandwich ELISA technique was employed to quantify the tumor necrosis factor (TNF)-α, interleukin (IL)-1β, caspase-3, caspase-9, matrix metalloproteinase (MMP)-9, peroxisome proliferator-activated receptor-γ coactivator (PGC)-1α, monocyte chemoattractant protein-1 (MCP-1), carnitine acetyltransferase, and endothelial nitric oxide synthase (eNOS) levels, in the rat brain samples. A standard curve of different biomarkers was plotted to estimate TNF-α (pg/ml), IL-1β (pg/ml), caspase-3/-9 (ng/ml), eNOS (pg/ml), carnitine acetyltransferase, MMP-9 (ng/ml), PGC-1α (ng/ml), and MCP-1 (ng/ml) in the samples. The concentration of GABA and glutamate were assessed by using high-performance liquid chromatography-fluorescence detector (HPLC-FLD) technique (Kumar et al., 2021).

2.13. Estimation of mitochondrial respiratory chain functions in the brain

NADH dehydrogenase (complex I) (King and Howard, 1967), succinate dehydrogenase (complex II) (King et al. 1976), cytochrome oxidase (complex IV) (Sottocasa et al. 1967), and F1F0 synthase (complex V) (Fiske and Subbarow, 1925; Griffiths and Houghton, 1974) were quantified to assess the activity of mitochondrial respiratory chain. Citrate synthase activity was measured by following the method of Coore et al. (1971). Cytochrome c was assessed by the method given by Perez-Pinzon et al. (1999).

2.14. Evaluation of MTT reduction

Dehydrogenase enzymes in the mitochondrial assay mixture reduce MTT to blue formazan that depicts mitochondrial functionality (Liu et al., 1997). MTT (0.1 mg/ml) and mitochondrial suspension was incubated (37 °C for 30 min) and centrifuged (2000 × *g*). Absolute ethanol and formazan pellet mixture was re-centrifuged 10 min and supernatant was removed whose absorbance was measured at λ_{max} = 595 nm. MTT reduction is stated as μg formazan formed/min/mg protein and the data was normalized to citrate synthase activity.

2.15. Estimation of mitochondrial permeability transition

Mitochondrial swelling and contraction (Tedeshi and Harris, 1958) and mitochondrial membrane potential (MMP) (Cassarino et al., 1999) were noted to assess mitochondrial permeability transition (MPT) (Varibro et al., 2001).

2.16. Evaluation of Adenine (ATP and ADP)

nucleotide levels

Freezing brain tissue was added to a micro-centrifuge tube (2.0 ml) along with perchloric acid (0.4 M) and instantly homogenized. The homogenate was ice-cooled (35 min). It was centrifuged (14,000 × *g* at 4 °C). K_2CO_3 (4 M) was added to the supernatant which was again cooled for 12 min at −80 °C for precipitation of the perchlorate. The assay mixture was re-centrifuged. Supernatant was stored at −80 °C for high-performance liquid chromatography (HPLC) analysis. The sample and standard were added discretely to the HPLC column. Elution was observed at λ_{max} = 254 nm, at a flow rate of 2 ml/min using Supelcosil LC-18, 5 µm (15 cm × 0.46 cm) reversed phase column (Supelco, Crans, Switzerland). An isocratic elution of the samples was executed with 0.52 µm KH_2PO_4 buffer (pH 4.0), containing 1.25% (v/v) methanol and 0.04% tetrabutylammonium phosphate. Peaks were recognized by their retention period and by means of co-chromatography with standards. ATP and ADP levels was represented as nmol/mg protein (Victor et al. 1987).

2.17. Estimation of brain acetylcholinesterase (AChE) activity

The supernatant (0.05 ml), 0.1 M phosphate buffer (pH 8, 3 ml), 0.05 M Ellman's reagent (0.1 ml) and 0.075 M acetylthiocholine iodide (0.1 ml) were taken and the absorbance of yellow colored chromophore was spectrophotometrically (λ_{max}=412 nm) determined for 2 min at 30 s interval. The rate at which absorbance changes per min was determined [ΔA_{412}/min = {A_{412}(time 2) – A_{412}(time 1) / {Time 2 – Time 1}]. Molar extinction coefficient of the chromophore (ε=1.36 × 10^4 $M^{-1}cm^{-1}$ at 412 nm) was used for calculation of AChE activity (μmol acetylthiocholine iodide (AThCh) hydrolysed/min/mg protein) (Ellman et al., 1961).

2.18. Brain histology

10% neutral buffered formalin solution (10% NBF) was administered *via* left ventricle through a gravity fed perfusion setup in anesthetized animals. Brain tissues were fixed in 10:1 ratio using 10% NBF and 0.05% sodium azide (pH 7.1) and stored at 4°C for histology (Zaborszky et al., 2006). 5.0 μm sections were carved out and stained with hematoxylin and eosin (H&E). DPX-resin mounting medium was used to prepare slides. Slides were analyzed using light microscopy (× 40).

2.19. Statistical analysis

Data will be scrutinized by a knowledgeable researcher, blinded to diverse treatments of rat cohorts. Grubb's test was used to detect outliers. Kolmogorov-Smirnov test was used to assess the normal distribution and Levene's test disclosed homogeneity of variance (HOV $p > 0.05$). Data was examined by one-way ANOVA and Tukey's *posthoc* test. Time dependent data of mean body weight, feed/water intake, locomotor activity, motor coordination, and escape latency in MWM acquisition trials was analyzed by repeated measures two-way ANOVA and Bonferroni's *posthoc* test. Data stated as mean ± S.E.M. A p value less than 0.05 is considered to be statistically significant.

3. Results

3.1. Nesfatin-1 attenuated LM-induced rise in mean body weight, food intake, and water intake

LM administration for 8 weeks in sham rats caused a significant ($p < 0.001$) increase in mean body weight, feed, and water intake in comparison to sham rats that were given vehicle only. However, nesfatin-1 (0.3, 1, and 3 μg/kg, ICV) treatment significantly ($p < 0.001$) attenuated LM-induced rise in mean body weight, feed, and water intake of rats in comparison to rats that were given LM only. ICV administration of nesfatin-1 *per se* also decreased ($p < 0.001$) the mean body weight, feed, and water intake of rats with respect to sham rats that were given vehicle alone. Administration of piracetam (a nootropic drug) attenuated ($p < 0.001$) the LM-induced rise in the mean body weight, feed, and water intake of rats in comparison to rats that were given LM only (Fig. 1).

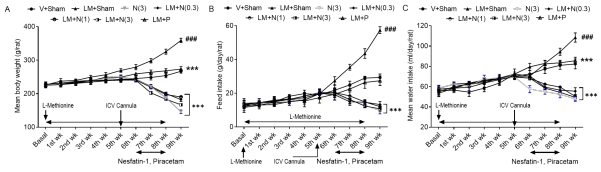

Fig. 1 Nesfatin-1 attenuated (A) mean body weight, (B) mean food intake, and (C) mean water intake (n = 8). ### $p < 0.001$ *vs.* V+Sham, *** $p < 0.001$ *vs.* LM+Sham. V: Vehicle, LM: L-Methionine, N: Nesfatin-1

3.2. Nesfatin-1 had no effect on the locomotor activity

and motor co-ordination

There was no significant ($p > 0.05$) difference in the mean locomotor activity and motor coordination among different groups in response to diverse drug treatments (Fig. 2)**.**

3.3. Nesfatin-1 increased learning and memory of rats in Morris water maze and novel object recognition task (NORT) in LM rat model of VCID

The MEL of different groups showed no significant ($p > 0.05$) difference from day 1 to 3; however, significant inter-group variation was observed on day 4 during the acquisition trials (Fig 2C). On day 4, administration of LM in sham rats caused a significant ($p < 0.01$) increase in the MEL of rats with respect to the vehicle treated sham rats. V+Sham and N(3) *per se* groups exhibited marked ($p < 0.001$) reduction in MEL on day 5 with respect to that of day 1. On day 5, we observed that administration of piracetam (standard drug) for 14 days in LM treated rats caused a significant ($p < 0.001$) fall in MEL when compared to administration of LM in sham rats. Interestingly, ICV administration of nesfatin-1 (0.3, 1, and 3 μg/kg) in LM treated rats decreased ($p < 0.05$, $p < 0.01$, $p < 0.001$) the MEL with respect to rats that received LM alone. N(3) *per se* group exhibited no significant variation in the MEL with respect to V+Sham group.

During probe trial on day 6, administration of LM for 8 weeks significantly ($p < 0.001$) decreased the TSTQ when compared to sham rats that received vehicle alone. ICV administration of nesfatin-1 (0.3, 1, and 3 μg/kg) in LM treated rats augmented the TSTQ ($p < 0.01$, $p < 0.001$, $p < 0.001$) with respect to rats that were subjected to LM treatment alone. Piracetam significantly ($p < 0.001$) elevated the TSTQ in LM treated rats (Fig 2D). N(3) *per se* group showed significant ($p < 0.001$) increase in TSTQ with respect to LM+Sham group, however, no significant ($p > 0.05$) variation was noticed with respect to V+Sham group. Nesfatin-1 (1 and 3 μg/kg, ICV) caused a significant increase ($p < 0.001$) in TSTQ in comparison to nesfatin-1 (0.3 μg/kg, ICV) in LM rat model of VCID.

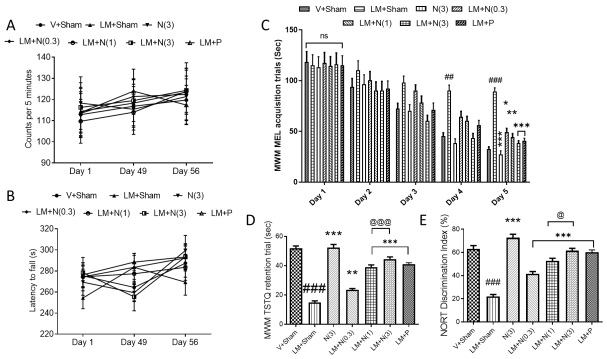

Fig. 2 Nesfatin-1 attenuated LM-induced symptoms of dementia in rats and had no significant effect on locomotor activity and motor co-ordination. Effect of nesfatin-1 on (A) locomotor activity, (B) motor co-ordination, (C) mean escape latency (MEL) in MWM acquisition trials, (D) Time spent in target quadrant (TSTQ) in MWM retention trial, and (E) % discrimination index (DI) in NORT ($n = 8$). $^{\#\#}$ $p < 0.01$, $^{\#\#\#}$ $p < 0.001$ *vs.* V+Sham, * $p < 0.05$, ** $p < 0.01$, *** $p < 0.001$ *vs.* LM+Sham, $^{@}$ $p < 0.05$, $^{@@@}$ $p < 0.001$ *vs.* LM+N(0.3). V: Vehicle, LM: L-Methionine, N: Nesfatin-1

In the NORT, administration of LM for 8 weeks significantly ($p < 0.001$) lowered the % discrimination index (DI) in comparison to vehicle treated sham rats. Administration of nesfatin-1 (ICV) for 14 days significantly ($p < 0.001$, $p < 0.001$, $p < 0.001$) increased the %DI in LM treated rats with respect to rats that received LM alone. Piracetam treated group showed a significant ($p < 0.001$) rise in %DI when compared to LM+Sham group. N(3) *per se* group showed a significant increase ($p < 0.001$) in the %DI with respect to the LM+Sham group, however, no significant variation ($p > 0.05$) was observed in comparison to the V+Sham group (Fig. 2E). Nesfatin-1 (1 and 3 μg/kg, ICV) caused a significant increase ($p < 0.05$) in %DI in comparison to nesfatin-1 (0.3 μg/kg, ICV) in LM rat model of VCID.

3.4. Nesfatin-1 attenuated serum homocysteine (Hcy) levels, total nitrites, and lipoproteins in LM rat model of VCID

Administration of LM in sham rats for 8 weeks amplified ($p < 0.001$) the serum HCy levels, total nitrites, TC, TGs, LDL-C, and VLDL levels and decreased ($p < 0.001$) HDL-C levels when compared with vehicle treated sham

rats. Treatment of LM administered rats with nesfatin-1 (0.3, 1, and 3 μg/kg, ICV) for 2 weeks significantly diminished the serum HCy ($p < 0.05$, $p < 0.001$, $p < 0.001$), nitrites content ($p < 0.05$, p , 0.01, $p < 0.001$), TC ($p < 0.05$, $p < 0.001$, $p < 0.001$), TGs ($p < 0.01$, $p < 0.01$, $p < 0.001$), LDL ($p > 0.01$, $p < 0.001$, $p < 0.001$), and VLDL levels ($p < 0.05$, $p < 0.05$, $p < 0.001$) and increased HDL levels ($p > 0.05$, $p > 0.001$, $p < 0.001$) with respect to rats that received LM alone. In LM treated rats, administration of piracetam significantly ($p < 0.001$) diminished the serum HCy, nitrites content, TC, TGs, LDL-C, and VLDL levels and increased HDL-C levels with respect to rats that received LM alone (Fig. 3). N(3) *per se* group showed a significant decrease in serum HCy ($p < 0.001$), nitrites content ($p < 0.001$), TC ($p < 0.001$), TG ($p < 0.001$), LDL ($p < 0.001$), and VLDL levels ($p < 0.001$) and increase in HDL levels ($p < 0.05$) with respect to LM+Sham group, however, the increase in HDL level was significantly less ($p < 0.001$) with respect to the V+Sham group. The current data showed that nesfatin-1 (3 μg/kg, ICV) caused a significant amelioration in the levels of blood biomarkers (HCy, total nitrites, TC, TGs, LDL-C, VLDL, and HDL-C) in comparison to nesfatin-1 (doses 0.3 and/or 1 μg/kg, ICV) in LM rat model of VCID.

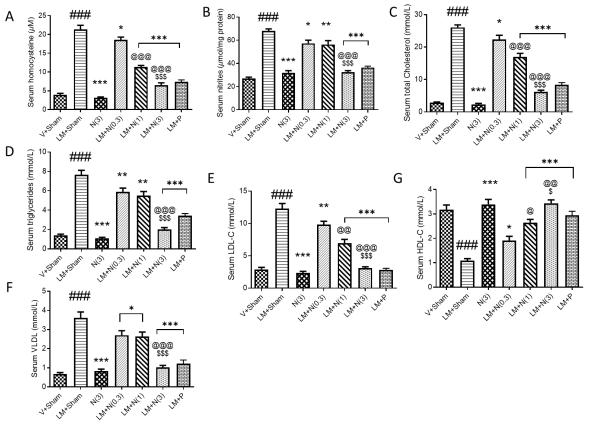

Fig. 3 Nesfatin-1 ameliorated levels of serum hmocysteine, total nitrites, and dyslipidaemia in LM rat model of VCID A) homocysteine, B) total nitrites, C) total cholesterol, D) triglycerides, E) LDL-C, F) VLDL, and G) HDL-C ($n = 8$) $^{###}$ $p < 0.001$ *vs.* V+Sham, * $p < 0.05$, ** $p < 0.01$, *** $p < 0.001$ *vs.* LM+Sham, $^{@}$ $p < 0.05$, $^{@@}$ $p < 0.01$, $^{@@@}$ $p < 0.001$ *vs.* LM+N(0.3), $^{\$}$ $p < 0.05$, $^{\$\$\$}$ $p < 0.001$ *vs.* LM+N(1). Hcy: Homocysteine, TC: Total cholesterol, TG: Triglycerides, LDL-C: Low-density lipoprotein cholesterol, VLDL: Very low-density lipoproteins, HDL-C: High-density lipoprotein cholesterol, V: Vehicle, LM: L-Methionine, N: Nesfatin-1

3.5. Nesfatin-1 attenuated mitochondrial oxidative stress in the brain of LM treated rats

Oral administration of LM in sham rats for 8 weeks daily significantly amplified ($p < 0.001$) the mitochondrial TBARS and protein carbonyls levels and decreased SOD, catalase activity, and GSH levels when compared to the vehicle treated sham rats. Treatment of LM administered rats with nesfatin-1 (0.3, 1, and 3 μg/kg, ICV) diminished mitochondrial TBARS ($p < 0.05$, $p < 0.05$, $p < 0.001$) and protein carbonyls levels ($p < 0.05$, $p < 0.01$, $p < 0.001$) and enhanced SOD ($p > 0.05$, $p < 0.001$, $p < 0.001$), catalase ($p < 0.001$, $p < 0.001$, $p < 0.001$), and GSH levels ($p > 0.05$, $p < 0.01$, $p < 0.001$) with respect to rats that received LM alone. In LM administered rats, treatment with piracetam conspicuously declined mitochondrial TBARS ($p < 0.001$) and protein carbonyls levels ($p < 0.001$) and enhanced SOD ($p < 0.001$), catalase ($p < 0.001$), and GSH levels ($p < 0.001$) with respect to rats that received LM only (Fig. 4). N(3) *per se* group showed a significant decrease in brain TBARS ($p < 0.001$) and protein carbonyls ($p < 0.001$) and an increase in SOD ($p < 0.001$), catalase ($p < 0.001$), and GSH levels ($p < 0.001$) with respect to rats that received LM alone, however, no significant variation was noticed ($p > 0.05$) with respect to the V+Sham group. The current data showed that nesfatin-1 (3 μg/kg, ICV) caused a significant amelioration in the levels of brain biomarkers of oxidative stress (TBARS, SOD, catalase, and protein carbonyls) in comparison to nesfatin-1 (doses 0.3 and/or 1 μg/kg, ICV) in LM rat model of VCID.

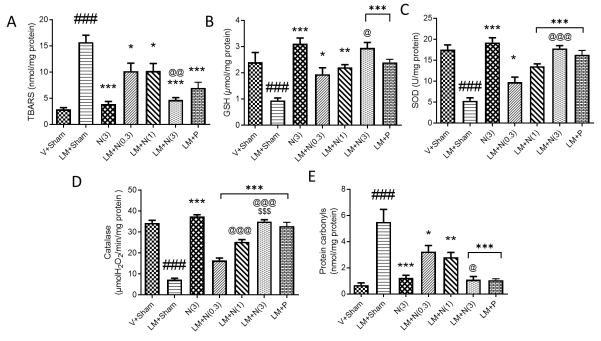

Fig. 4 Nesfatin-1 ICV treatment for 14 days ameliorated biomarkers of oxidative stress in the mitochondrial fraction of the brain of LM treated rats A) Thiobarbituric acid reactive substances (TBARS), B) Glutathione (GSH), C) Superoxide dismutase (SOD), D) Catalase, and E) Protein carbonyls (n = 5) $^{###}$ $p < 0.001$ *vs.* V+Sham, * $p < 0.05$, ** $p < 0.01$, *** $p < 0.001$ *vs.* LM+Sham, $^{@}$ $p < 0.05$, $^{@@}$ $p < 0.01$, $^{@@@}$ $p < 0.001$ *vs.* LM+N(0.3), $^{\$\$\$}$ $p < 0.001$ *vs.* LM+N(1). V: Vehicle, LM: L-Methionine, N: Nesfatin-1

3.6. Nesfatin-1 restored the mitochondrial activity in the brain of LM treated rats

Administration of LM orally in sham rats for 8 weeks decreased ($p < 0.001$) the mitochondrial respiratory enzymes (in electron transport chain) activity (Complex I, II, IV, and F1F0ATPase) when compared with vehicle treated sham rats. Furthermore, LM caused a significant ($p < 0.001$) decrease in MTT reduction, ATP levels, and an increase in ADPs in rats with respect to the rats that were given vehicle and sham surgery. Treatment of LM administered rats with nesfatin-1 (0.3, 1, and 3 μg/kg, ICV) for 14 days significantly enhanced the activity of Complex I ($p < 0.001$, $p < 0.001$, $p < 0.001$), II ($p < 0.01$, $p < 0.001$, $p < 0.001$), IV ($p < 0.001$, $p < 0.001$, $p < 0.001$), and F1F0ATPase ($p > 0.05$, $p < 0.01$, $p < 0.001$) with respect to rats that received LM alone. Nesfatin-1 (0.3, 1, and 3 μg/kg, ICV) attenuated LM-induced decrease in MTT reduction ($p > 0.05$, $p < 0.001$, $p < 0.001$), ATPs ($p < 0.05$, $p < 0.05$, $p < 0.001$), and attenuated the increase in ADPs ($p < 0.01$, $p < 0.001$, $p < 0.001$) in the brain of rats with respect to rats that received LM only. In LM treated rats, oral treatment with piracetam for 2 weeks conspicuously ($p < 0.001$) elevated mitochondrial respiratory enzymes activity (Complex I, II, IV, and F1F0ATPase), MTT reduction, ATP levels, and decreased ADPs with respect to rats that were given LM only (Table 1). N(3) *per se* group showed a significant increase ($p < 0.001$) in the brain Complex I, II, IV, and F1F0ATPase activities with respect to rats that received LM alone, however, no significant variation was noticed ($p > 0.05$) with respect to the V+Sham group. Furthermore, N(3) *per se* group exhibited enhanced MTT reduction ($p < 0.001$), ATPs ($p < 0.001$), and a decrease in ADPs ($p < 0.001$) in comparison to rats that received LM alone, however, no significant variation was noticed ($p > 0.05$) with respect to the V+Sham group.

Table 1 Effect of nesfatin-1 ICV treatment on the mitochondrial functions in LM rat model of VCID.

Parameter / Group	V+Sham	LM+Sham	N(3)	LM+N(0.3)	LM+N(1)	LM+N(3)	LM+P
Complex I (nmol NADH oxidized/min/mg protein)	107.2 ± 1.522	31.39 ± 2.191 $^{###}$	109.4 ± 2.05 ***	57.79 ± 3.584 ***	77.54 ± 3.906 *** $^{@@@}$ $^{\$\$\$}$	100.9 ± 2.521 *** $^{@@@}$ $^{\$\$\$}$	93.59 ± 3.137 ***
Complex II (nmol succinate oxidized/min/mg protein)	154.6 ± 4.515	66.91 ± 4.207 $^{###}$	161.8 ± 4.973 ***	94.9 ± 4.675 **	135.9 ± 3.369 *** $^{@@@}$	162.4 ± 3.726 *** $^{@@}$ $^{\$\$\$}$	155.8 ± 4.764 ***
Complex IV (nmol cytochrome c oxidized/min/mg protein)	148.4 ± 3.053	42.85 ± 4.39 $^{###}$	156.8 ± 3.861 ***	66.95 ± 3.164 ***	92.95 ± 3.049 *** $^{@@@}$	121.0 ± 2.315 *** $^{@@@}$ $^{\$\$\$}$	106.5 ± 2.055 ***
F1F0ATPase (nmol ATP hydrolyzed/min/mg protein)	15.44 ± 1.131	6.78 ± 1.073 $^{###}$	18.11 ± 1.073 ***	12.10 ± 1 *	12.7 ± 0.7375 **	15.77 ± 1.149 ***	14.68 ± 1.231 ***
Mitochondrial swellin	0.3029 ±	0.857 ±	0.2385±	0.6637 ± 0.04	0.5041 ±	0.2155 ±	0.2839 ±

g (absorbance at 520 nm)	0.030 09	0.0376 4 ###	0.0228 9 ***	829 **	0.0404 1 *** @	0.0239 2*** @@ @ $$$	0.0318 ***
Scattering at 540 nm	80.83 ± 2.178	29.48 ± 3.075 ###	81.02 ± 4.439 ***	46.08 ± 1.94 **	57.09 ± 2.368 ***	80.61 ± 2.798 *** @@ @ $$$	79.9 ± 0.6864 ***
Mitochondrial membrane potential (fluorescence intensity)	826.6 ± 20.69	277.9 ± 11.2 ###	847.2 ± 17.88 ***	374.1 ± 16.54 **	556.7 ± 16.56 *** @@ @	761.9 ± 11.71 *** @@ @ $$$	733.7 ± 11.57 ***
Citrate synthase (nmol/min/mg protein)	61.27 ± 3.314	167.2 ± 6.165 ###	48.67 ± 3.035 ***	135.9 ± 3.532 ***	104.3 ± 2.288 *** @@ @	65.82 ± 4.554 *** @@ @ $$$	67.57 ± 2.791 ***
Carnitine acetyltransferase (ng/ml)	14.95 ± 1.719	66.5 ± 2.084 ###	15.53 ± 1.756 ***	53.51 ± 2.894 **	47.8 ± 1.908 ***	20.72 ± 1.317 *** @@ @	22.72 ± 1.945 ***
MTT reduction (μg formazan formed/min/mg protein)	7.896	1.397	8.32	3.212 ± 0.387	5.103 ± 0.1343 ###	8.582 ± 0.6223 ***	7.7340 ± 0.2726 *
Cytochrome *c* (nmol/mg protein)	2.389 ± 0.3823	15 ± 1.073 ###	1.679 ± 0.1991 ***	11.52 ± 0.4996 **	8.028 ± 0.4654 *** @@	3.351 ± 0.3633 *** @@ @ $$$	4.243 ± 0.318 ***
ATP (nmol/mg protein)	14.39 ± 1.65	1.815 ± 0.3848 ###	15.52 ± 1.24 ***	7.185 ± 1.042 *	7.315 ± 0.8273 *	10.77 ± 0.7458 ***	9.28 ± 1.129 ***
ADP (nmol/mg protein)	4.3 26 ± 0.8 09 6	10.81 ± 0.5887 ###	2.501 ± 0.4214 ***	7.527 ± 0.6233 **	6.572 ± 0.2653 ***	4.587 ± 0.1021 *** @@	5.783 ± 0.8336 ***

($n = 5$) ### $p < 0.001$ *vs.* V+Sham, * $p < 0.05$, ** $p < 0.01$, *** $p < 0.001$ *vs.* LM+Sham, @ $p < 0.05$, @@ $p < 0.01$, @@@ $p < 0.001$ *vs.* LM+N(0.3), $ $p < 0.05$, $$ $p < 0.01$, $$$ $p < 0.001$ *vs.* LM+N(1). V: Vehicle, LM: L-Methionine, N: Nesfatin-1

Furthermore, we observed the effects of nesfatin-1 on mitochondrial permeability transition, mitochondrial swelling, and mitochondrial membrane potential. The following parameters were measured from isolated Percoll-gradient purified rat brain mitochondria to show the direct effect of ICV nesfatin-1 treatment in inducing mitochondrial permeability transition: mitochondrial swelling, membrane potential dissipation, and

cytochrome *c* release. The reduction in the reflectance of light at λ_{max} = 540 nm indicated high-amplitude swelling of the mitochondria as a result of the permeability transition. Treatment with LM induced a significant ($p < 0.001$) swelling in isolated brain mitochondria substantiated by a decrease ($p < 0.001$) in light scattering/reflectance at λ_{max} = 540 nm with respect to treatment with vehicle alone. In the present study, LM treated rats' mitochondria showed degenerated membrane potential, as spotted by the release of the membrane potential sensitive dye, Rh123 from the brain mitochondria subsequent to the initiation of permeability transition. In comparison to vehicle treated sham rats, treatment of rats with LM caused a significant ($p < 0.001$) dissipation of membrane potential of mitochondria in the brain. This degeneration of membrane potential was significantly ($p < 0.01$, $p < 0.001$, $p < 0.001$) inhibited by ICV administered nesfatin-1 at doses 0.3, 1, and 3 μg/kg. Oral administration of piracetam also attenuated ($p < 0.001$) LM-induced mitochondrial swelling and dissipation of membrane potential.

Substrates (*e.g.*, acetyl-coenzyme A) that would otherwise be blocked from entering the mitochondrial matrix by the inner mitochondrial membrane are made possible by the opening of the permeability transition pore. It made it possible to use a straightforward enzyme assay to show how the permeability hole opened. Acetyl coenzyme A injected externally allows citrate synthase and carnitine acyltransferase activity to be measured, indicating the permeability pore opening. In this study, LM administration caused a significant ($p < 0.001$) rise in the brain carnitine acetyltransferase and citrate synthase activity with respect to vehicle treated sham rats. ICV injection of nesfatin-1 (0.3, 1, and 3 μg/kg) prevented the LM-induced rise in carnitine acetyltransferase ($p < 0.01$, $p < 0.001$, $p < 0.001$) and citrate synthase ($p < 0.001$, $p < 0.001$, $p < 0.001$) activity with respect to LM treated rats. Release of cytochrome *c* from the mitochondrial intermembrane space following permeability transition was detected. LM administration caused a significant ($p < 0.001$) rise in cytochrome *c* levels with respect to vehicle treated sham rats. ICV injection of nesfatin-1 (0.3, 1, and 3 μg/kg) prevented the LM-induced rise in cytochrome *c* ($p < 0.01$, $p < 0.001$, $p < 0.001$) levels with respect to LM treated rats (Table 2). Piracetam caused a significant decrease in carnitine acetyltransferase ($p < 0.001$), citrate synthase ($p < 0.001$) activity, and cytochrome *c* levels ($p < 0001$) with respect to L-Met treated rats.

Furthermore, L-Met caused a significant ($p < 0.001$) rise in the ADPs and decrease in the ATP levels with respect to the vehicle treated sham rats. ICV administration of nesfatin-1 significantly attenuated L-Met-induced rise in the ADPs ($p < 0.001$, $p < 0.001$, $p < 0.001$) and decrease in the ATP levels ($p < 0.01$, $p < 0.001$, $p < 0.001$) with respect to the L-Met alone treated rats. Treatment with piracetam in L-Met administered rats caused a significant ($p < 0.001$) increase in the brain ATPs and a decrease in ADPs in comparison to L-Met alone treated rats (Table 1). The current data showed that nesfatin-1 (3 μg/kg, ICV) caused a significant amelioration of mitochondrial functions in comparison to nesfatin-1 (doses 0.3 and/or 1 μg/kg, ICV) in LM rat model of VCID.

3.7. Nesfatin-1 ameliorated parameters of neuroinflammation, apoptotic markers, PGC-1α, and eNOS

Oral administration of LM in sham rats for 8 weeks daily significantly amplified ($p < 0.001$) TNF-α, IL-1β, MCP-1, MMP-9, MPO, caspase-3 and caspase-9 levels and decreased eNOS and PGC-1α expression when compared to the vehicle treated sham rats. Treatment of LM administered rats with nesfatin-1 (0.3, 1, and 3 μg/kg, ICV) for 14 days diminished TNF-α ($p < 0.001$, $p < 0.001$, $p < 0.001$), IL-1β ($p > 0.05$, $p < 0.001$, $p < 0.001$), MCP-1 ($p < 0.05$, $p < 0.001$, $p < 0.001$), MMP-9 ($p < 0.01$, $p < 0.001$, $p < 0.001$), MPO ($p > 0.01$, $p < 0.01$, $p < 0.001$), caspase-3 ($p < 0.001$, $p < 0.001$, $p < 0.001$), and caspase-9 ($p < 0.001$, $p < 0.001$, $p < 0.001$) levels and enhanced eNOS ($p < 0.05$, $p < 0.001$, $p < 0.001$) and PGC-1α levels ($p < 0.01$, $p < 0.001$, $p < 0.001$) with respect to rats that received LM alone. In LM administered rats, treatment with piracetam noticeably declined TNF-α ($p < 0.001$), IL-1β ($p < 0.001$), MCP-1 ($p < 0.001$), MMP-9 ($p < 0.001$), MPO ($p < 0.01$), caspase-3 ($p < 0.001$), and caspase-9 ($p < 0.001$) levels and enhanced eNOS ($p < 0.001$) and PGC-1α levels ($p < 0.001$) with respect to rats that received LM only (Table 2). N(3) *per se* group disclosed a significant ($p < 0.001$) decrease in brain TNF-α, IL-1β, MCP-1, MMP-9, MPO, caspase-3, and caspase-9 levels and enhanced eNOS and PGC-1α levels with respect to rats that received LM alone, however, no significant variation was noticed ($p > 0.05$) with respect to the V+Sham group. The current data showed that nesfatin-1 (3 μg/kg, ICV) caused a

significant amelioration in the levels of brain biomarkers of inflammation, apoptosis, eNOS, and PGC-1α in comparison to nesfatin-1 (doses 0.3 and/or 1 μg/kg, ICV) in LM rat model of VCID.

Table 2 Effect of nesfatin-1 ICV treatment for 14 days on the inflammatory biomarkers, apoptotic markers, PGC-1α, and eNOS in LM rat model of VCID.

Parameter / Group	V+Sham	LM+Sham	N(3)	LM+N(0.3)	LM+N(1)	LM+N(3)	LM+P
TNF-α (pg/ml)	13.24 ± 0.5352	61.55 ± 2.048 ###	16.62 ± 0.7929***	42.666 ± 1.622 ***	34.89 ± 1.044 *** @	20.86 ± 1.811 *** @@@ $$$	23.7 ± 2.038 ***
IL-1β (pg/ml)	0.5418 ± 0.1621	3.555 ± 0.375 ###	0.4913 ± 0.1282 ***	2.549 ± 0.3834	1.676 ± 0.2426 ***	1.011 ± 0.282 *** @	1.457 ± 0.2436 ***
MCP-1 (pg/ml)	21.72 ± 1.145	114.8 ± 5.536 ###	20.53 ± 1.66 ***	93.27 ± 5.679 *	67.14 ± 5.877 *** @@	35.39 ± 3.931 *** @@@ $$$	37.35 ± 2.016 ***
MMP-9 (ng/ml)	10.33 ± 0.4371	26.24 ± 1.971 ###	8.012 ± 1.073 ***	17.79 ± 1.992 **	14.25 ± 1.131 ***	8.826 ± 1.173 ***	12.25 ± 2.11 ***
Myelo peroxidase (U/mg protein)	10 4 ± 0.0 55 84	11 ± 0.3 444 ###	46 7 ± 0.0 39 86 ***	16 ± 0.16 8 **	85 ± 0.1 083 **	543 ± 0.3 328 ***	46 5 ± 0.0 24 96 ***
eNOS (pg/ml)	18.97 ± 2.135	4.389 ± 0.6922 ###	19.92 ± 1.533 ***	11.23 ± 1.87 *	17 ± 1.427 ***	20.4 ± 1.007 *** @@	21.3 ± 0.8234 ***
PGC-1α (ng/ml)	76.82 ± 5.143	17.82 ± 1.413 ###	87.26 ± 4.483 ***	37.32 ± 3.445 **	54.13 ± 3.427 ***	75.95 ± 4.468 *** @@	71.41 ± 3.926 ***
Caspase-3 (ng/ml)	2.922 ± 0.341	10.98 ± 0.5108 ###	1.698 ± 0.2174 ***	7.095 ± 0.501 ***	4.453 ± 0.276 *** @@@	2.465 ± 0.3653 *** @@ @ $	2.509 ± 0.3259 ***
Caspase-9 (ng/ml)	1.129 ± 0.1739	8.667 ± 0.3642 ###	0.771 ± 0.0819 ***	5.723 ± 0.2689 ***	3.71 ± 0.3507 *** @@@	1.628 ± 0.2577 *** @@@ $$$	2.346 ± 0.2866 ***

(n = 5) ### $p < 0.001$ *vs.* V+Sham, * $p < 0.05$, ** $p < 0.01$, *** $p < 0.001$ *vs.* LM+Sham, @ $p < 0.05$, @@ $p < 0.01$, @@@ $p < 0.001$ *vs.* LM+N(0.3), $ $p < 0.05$, $$ $p < 0.01$, $$$ $p < 0.001$ *vs.* LM+N(1). V: Vehicle, LM: L-Methionine, N: Nesfatin-1

3.8. Nesfatin-1 ameliorated GABA and glutamate levels and acetylcholinesterase activity in LM rat model of VCID

HPLC-FLD data exhibited that LM administration (*p.o.*) in sham rats, significantly augmented ($p < 0.001$) glutamate and AChE activity and decreased GABA levels when compared to the vehicle treated sham rats. Treatment of rats with nesfatin-1 (0.3, 1, and 3 μg/kg, ICV) attenuated LM-induced rise in glutamate ($p < 0.01$, $p < 0.01$, $p < 0.001$) and AChE activity ($p < 0.01$, $p < 0.001$, $p < 0.001$) and also enhanced GABA levels ($p < 0.05$, $p < 0.05$, $p < 0.001$) with respect to rats that received LM alone. In LM administered rats, treatment with piracetam noticeably ($p < 0.001$) declined glutamate and AChE activity and enhanced GABA levels with respect to rats that received LM only. N(3) *per se* group displayed a significant ($p < 0.001$) decrease in brain glutamate levels and AChE activity and enhanced GABA levels with respect to rats that received LM alone, however, no significant variation was noticed ($p > 0.05$) with respect to the V+Sham group (Fig. 5).

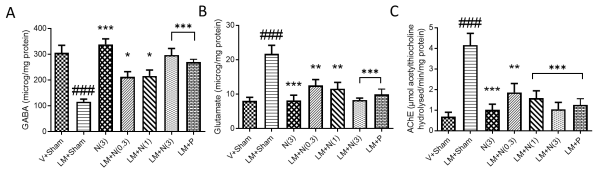

Fig. 5 Nesfatin-1 attenuated LM-induced dysfunctions in neurotransmitter levels, A) GABA, B) Glutamate, C) acetylcholinesterase (AChE) activity, in the brain of rats ($n = 5$). $^{###}$ $p < 0.001$ *vs.* V+Sham, * $p < 0.05$, ** $p < 0.01$, *** $p < 0.001$ *vs.* LM+Sham. V: Vehicle, LM: L-Methionine, N: Nesfatin-1

3.9. Histopathological features of rat brain cortex and hippocampus

In histopathological analysis, the rats that were subjected to oral administration of LM and sham surgery showed significant neurodegenerative changes in the cortical and hippocampus area of the brain of rats. Pathological changes in the architecture of plasma membrane (such as blebbing), swelling, condensation of chromatin pyknosis (darkly stained nucleus), and cytoplasmic vacuolations were observed in the brain of rats of LM+Sham group. The sham rats showed no signs of neurodegeneration. Treatment of rats with nesfatin-1 (0.3, 1, and 3 μg/kg, ICV) for 14 days daily attenuated the LM-induced neuropathological changes. Nesfatin-1 reduced the condensation of genetic material and signs of alterations in plasma membrane. Nesaftin-1 attenuated LM triggered cytoplasmic vacuolations and darkly stained nuclei. Hence, it can be inferred that administration of nesfatin-1 ICV for 14 days in rats can attenuate the HHcy-triggered neurodegeneration in the brain (Fig. 6).

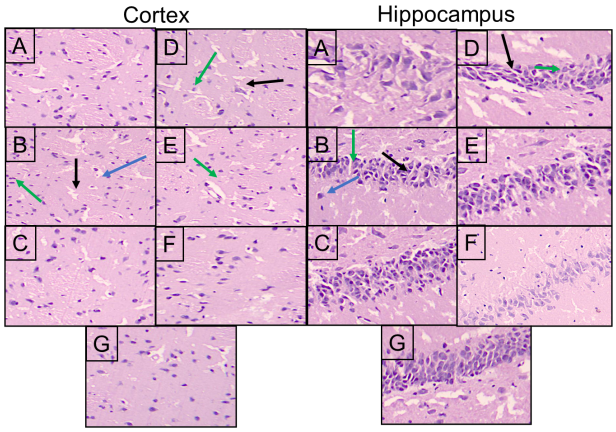

Fig. 6 Cortex and hippocampus regions of rat brain were used for histopathological analysis using H&E stain at × 40 magnification: A) V+Sham; B) LM+Sham; C) N(3) *per se*; D) LM+N(0.1); E) LM+N(1); F) LM+N(3); G) LM+P. Nesfatin-1 reduced neurodegenerative cells and apoptosis in the brain of rats against LM-induced neurotoxicity. Black arrow showing cytoplasmic vacuolation and blue arrow showing pyknosis were diminished by nesfatin-1 ICV treatment. Green arrow showing extravasation of neutrophils was attenuated by nesfatin-1 against LM-induced neutrophils accumulation in the brain regions. V: Vehicle, LM: L-Methionine, N: Nesfatin-1

4. Discussion

The present study provides comprehensive evidence that nesfatin-1 exerts potent neuroprotective and vasculoprotective effects in HHcy-induced VCID, primarily through preservation of mitochondrial function, suppression of oxidative and inflammatory cascades, and maintenance of endothelial integrity. HHcy is well recognized as a major modifiable risk factor for cerebrovascular injury, small-vessel disease, and dementia (Khan et al., 2018; Bhatia and Singh, 2021). Elevated Hcy levels have been shown to impair

endothelial NO signaling, induce oxidative damage, and disrupt neuronal energy metabolism pathological hallmarks recapitulated in our L-Met model and consistent with human VCID pathology (Kumar and Sandhir, 2020; Postnikova et al., 2025). The L-Met dose (1.7 g/kg/day for 8 weeks) employed in this study reliably produces sustained HHcy and associated cognitive deficits, as previously validated (Bhatia and Singh, 2021; Wang et al., 2020).

In the present study, L-Met oral administration for 8 weeks daily substantially increased serum Hcy, nitrites (i.e., nitrosative stress), and also caused dyslipidemia (elevated TC, TG, LDL, VLDL, and decreased HDL) which is a hallmark feature of vascular disturbances. L-Met triggered rise in oxidative markers such as TBARS and protein carbonyls in the brain. These findings are supported by prior studies demonstrating that Hcy promotes ROS generation through auto-oxidation and NADPH oxidase activation, leading to endothelial and neuronal injury (Kumar et al., 2021; Kumar and Sandhir, 2020). The observed deficits in spatial learning and memory align with evidence that HHcy impairs hippocampal synaptic plasticity and long-term potentiation (LTP), partly *via* NMDA receptor overstimulation and mitochondrial dysfunction (Suryavanshi et al., 2014; Kumar and Bansal, 2018; Postnikova et al., 2025).

A key finding of this study is the marked improvement in mitochondrial function following nesfatin-1 treatment. Mitochondrial dysfunction is a central mechanistic driver in the pathogenesis of VCID (Sandhir et al., 2012; Kumar and Sandhir, 2020). Excess Hcy induces mitochondrial oxidative stress, compromises respiratory chain complexes, disrupts ATP homeostasis, and promotes cytochrome-*c* release *via* opening of the mitochondrial permeability transition pore (Kumar and Sandhir, 2020; Sandhir et al., 2012). Nesfatin-1 (1 and 3 μg/kg, ICV) attenuated mitochondrial swelling, dissipation of membrane potential, and cytochrome-*c* release which are widely recognized indicators of protection against mitochondrial permeability transition. These results are strongly consistent with earlier studies demonstrating nesfatin-1's ability to enhance mitochondrial bioenergetics and reduce apoptosis (Varbiro et al., 2001). Zarrin et al. (2023) reported that nesfatin-1 activates PI3K/Akt signaling, thereby inhibiting mitochondrial pro-apoptotic pathways. Another study showed that nesfatin-1 regulates AMPK, a master energy sensor that improves mitochondrial oxidative phosphorylation (Dong et al., 2013; Yin et al., 2015). A study demonstrated that nesfatin-1 reduces mitochondrial ROS generation in models of ischemic brain injury (Yu et al., 2024). Our findings extend these results by showing that nesfatin-1 restores electron transport chain (ETC) complex activities (I, II, IV, V) and normalizes ATP/ADP ratio, suggesting enhanced metabolic stability that was critically hampered by L-Met. This is mechanistically relevant because impaired ETC activity and loss of ATP are primary drivers of cognitive decline in VCID and Alzheimer's-like pathologies. Restoration of mitochondrial function likely underlies the marked behavioral improvements observed in nesfatin-1–treated rats.

HHcy causes systemic and central oxidative overload, which triggers inflammatory signaling via NF-κB, NLRP3 inflammasome, and cytokine activation (Kumar and Bansal, 2018; Yu et al., 2024). In the present study, nesfatin-1 markedly reduced MPO activity and lowered IL-1β, TNF-α, and MCP-1 levels. These effects are supported by previous findings showing that nesfatin-1 suppresses NF-κB signaling and pro-inflammatory cytokine release in models of diabetic neuropathy and ischemic stroke (Fan et al., 2022; Yu et al., 2024). Nesfatin-1 reduces oxidative stress markers, including MDA and protein carbonyls, while boosting antioxidant enzymes such as SOD, catalase, and GSH (Solmaz et al., 2016). Our results mirror these outcomes, suggesting that nesfatin-1 exerts systemic antioxidative effects that stabilize neuronal and endothelial functions. The increase in reduced glutathione (GSH) and restoration of antioxidant enzyme activities indicate that nesfatin-1 enhances endogenous antioxidant defense, which is essential because mitochondrial ROS are central to progressing VCID pathology.

Endothelial dysfunction is a critical early event in VCID pathogenesis. Hcy is known to uncouple endothelial nitric oxide synthase (eNOS) and impair NO signalling, leading to endothelial dysfunction (Barutcigil and Tasatargi, 2018; Shah and Singh, 2006). Nesfatin-1 significantly reduced MMP-9 levels and enhanced eNOS expression, indicating protection against vascular injury. The ability of nesfatin-1 to reverse these abnormalities aligns with reports that nesfatin-1 enhances endothelial AMPK/eNOS activation and reduces vascular inflammation (Xu and Chen, 2020). The present data is supported findings by Zhou and Nao, 2024, who showed

that nesfatin-1 protects integrity of blood-brain barrier (BBB) in models of traumatic brain injury through modulation of tight junction proteins and oxidative defense pathways. The association between HHcy and MMP-9 activation is well documented; homocysteine disrupts the balance between MMP-9 and its tissue inhibitor TIMP-1 through epigenetic mechanisms involving DNA methylation (Mangat et al., 2014). Elevated MMP-9 contributes to extracellular matrix degradation, BBB disruption, and vascular remodelling in cerebral small vessel disease. The ability of nesfatin-1 to reduce MMP-9 levels in the present study represents an important vasculo-protective mechanism.

HHcy disrupts the cholinergic system and alters GABA–glutamate balance, contributing to cognitive deficits (Kumar et al., 2021; Postnikova et al., 2025). In the present study, L-Met administration significantly increased AChE activity and glutamate levels while decreasing GABA levels in the brain. Nesfatin-1 normalized AChE activity and restored neurotransmitter levels, indicating stabilization of synaptic transmission. This observation aligns with prior reports showing that nesfatin-1 modulates central neurotransmitter systems, particularly in the hippocampus, influencing learning and memory (Goebel-Stengel and Stengel, 2016). The interaction between Hcy and GABA receptors is particularly noteworthy; Hcy has been shown to act as an antagonist at GABA-A receptors, and GABA receptor agonists can ameliorate Hcy-induced vascular remodeling. The restoration of GABA levels by nesfatin-1 may therefore contribute to its neuroprotective effects.

The present study also investigated the involvement of key signalling pathways. Nesfatin-1 treatment significantly increased the levels of PGC-1α, a master regulator of mitochondrial biogenesis, as well as total and phosphorylated AMPK. These findings suggest that the mitochondrial protective effects of nesfatin-1 are mediated, at least in part, through activation of the AMPK/PGC-1α signalling pathways (Dong et al., 2013; Xu et al., 2018; Huang et al., 2022). PGC-1α activation promotes mitochondrial biogenesis and antioxidant defence, while AMPK acts as a cellular energy sensor that enhances oxidative phosphorylation and maintains energy homeostasis. The concurrent activation of these pathways by nesfatin-1 provides a mechanistic basis for its pleiotropic neuroprotective effects. Furthermore, nesfatin-1 treatment attenuated apoptotic markers, including caspase-3 and caspase-9 activation, consistent with inhibition of the mitochondrial apoptotic pathway (Yu et al., 2024; Zarrin et al., 2023). The reduction in cytochrome-c release from mitochondria to cytosol further supports the conclusion that nesfatin-1 preserves mitochondrial membrane integrity and prevents the initiation of apoptosis.

Histopathological examination of the brain cortex and hippocampus revealed that L-Met administration caused neurodegenerative changes, including plasma membrane blebbing, chromatin condensation, and neuronal swelling. Nesfatin-1 treatment, particularly at the higher doses (1 and 3 μg/kg), markedly attenuated these neuropathological alterations, confirming the structural correlates of the functional and biochemical improvements observed. Collectively, the findings suggest that nesfatin-1 provides neuroprotection through multiple mechanisms converging on mitochondrial stability *via* activation of AMPK and PGC-1α signaling, thereby supporting that mitochondrial survival and an increase in ATPs production are the key features that might improve the cognitive symptoms against L-Met-induced VCID. Stabilization of membrane potential prevents permeability transition and cytochrome-c release. Reduction of ROS generation diminishes inflammation and prevents vascular injury. Restoration of endothelial NO signaling supports cerebral perfusion, which is vital to preventing cognitive decline. Hence, the neuroprotective and vasculo-protective outcomes observed in the present study are consistent with the established role of nesfatin-1 as a metabolic and mitochondrial regulator.

The doses of nesfatin-1 employed in this study (0.3, 1, and 3 μg/kg, ICV) are consistent with previous reports demonstrating central effects of this peptide (Goebel et al., 2011; Dore et al., 2020; Shimizu et al., 2009; Mortazavi et al., 2015; Arabacı Tamer et al., 2022). The dose-dependent nature of the observed effects, with maximal protection at 3 μg/kg, supports the specificity of nesfatin-1-mediated neuroprotection. Piracetam, used as a standard nootropic agent, also attenuated L-Met-induced deficits, validating the experimental model and providing a reference for comparison. This study provides experimental evidence that nesfatin-1 directly targets and preserves mitochondrial homeostasis in HHcy-driven vascular cognitive impairment. The data identify nesfatin-1 as a mechanistically targeted modulator of mitochondrial bioenergetics and neurovascular integrity, supporting its development as a

candidate therapeutic for mitigating mitochondrial failure-mediated VCID. Further studies employing specific inhibitors of the AMPK and PGC-1α pathways would help to definitively establish the causal role of these signalling cascades in nesfatin-1-mediated neuroprotection. Additionally, long-term studies are warranted to evaluate the sustained efficacy and safety profile of nesfatin-1 in chronic models of VCID.

5. Conclusion

This study provides experimental evidence that nesfatin-1 directly targets and preserves mitochondrial homeostasis in HHcy-driven vascular cognitive impairment. In L-Met–treated rats, nesfatin-1 restored mitochondrial respiratory complex activities, stabilized membrane potential, prevented permeability transition, and suppressed cytochrome-*c* leakage, thereby maintaining ATP generation and preventing downstream neuronal injury. Biochemical levels, including normalisation of Hcy levels, reduction of lipid and protein oxidative adducts, restoration of redox balance, and attenuation of pro-inflammatory cytokine signalling accompanied these mitochondrial effects. Nesfatin-1 also improved endothelial reactivity and reduced MMP-9–associated vascular damage, indicating preserved neurovascular coupling. Additionally, these molecular and cellular corrections translated into significant improvements in spatial learning, memory consolidation, and recognition performance, confirming that nesfatin-1 effectively counteracts the cognitive sequelae of HHcy. Overall, the data identify nesfatin-1 as a mechanistically targeted modulator of mitochondrial bioenergetics and neurovascular integrity, supporting its development as a candidate therapeutic for mitigating mitochondrial failure–mediated VCID.

Acknowledgements

The authors are appreciative to M.M. College of Pharmacy, Maharishi Markandeshwar Deemed to be University, Mullana, Haryana; Swift School of Pharmacy, Ghaggar Sarai, Rajpura (Punjab), and Chitkara University, Punjab for facilitating the required research services.

Funding

This research did not receive any specific grant from funding agencies in the public, commercial, or not-for-profit sectors.

CRediT authorship contribution statement

Manish Kumar: Conceptualization, design of methodology, supervision, project administration, writing - review & editing. **Gaganjit Kaur:** Investigation. **Sushma Devi:** Writing - original draft. **Manish Shukla:** Data curation and resources.

Declaration of Competing Interest

The authors declare that they have no known competing financial interests or personal relationships that could have appeared to influence the work reported in this paper.

Availability of data and material

The data used to support the findings of this study are available.

Supplementary material 1

References

Alachkar A, Agrawal S, Baboldashtian M, Nuseir K, Salazar J, Agrawal A. L-methionine enhances neuroinflammation and impairs neurogenesis: Implication for Alzheimer's disease. J Neuroimmunol 2022;366:577843. https://doi.org/10.1016/j.jneuroim.2022.577843.

Arabacı Tamer S, Koyuncuoğlu T, Karagöz Köroğlu A, Akakın D, Yüksel M, Yeğen BÇ. Nesfatin-1 ameliorates oxidative brain damage and memory impairment in rats induced with a single acute epileptic seizure. Life Sci 2022;294:120376. https://doi.org/10.1016/j.lfs.2022.120376.

Barutcigil A, Tasatargil A. Effects of nesfatin-1 on atrial contractility and thoracic aorta reactivity in male rats. Clin Exp Hypertens 2018;40(5):414–20.

Bhatia P, Singh N. Ameliorative effect of ozagrel, a thromboxane A2 synthase inhibitor, in hyperhomocysteinemia-induced experimental vascular cognitive impairment and dementia. Fundam Clin Pharmacol 2021;35(4):650–66. https://doi.org/10.1111/fcp.12610.

Cassarino DS, Parks JK, Parker WD Jr, Bennett JP Jr. The parkinsonian neurotoxin MPP1 opens the mitochondrial permeability transition pore and releases cytochrome c in isolated mitochondria via an oxidative mechanism. Biochim Biophys Acta 1999;1453:49–62.

Chen LT, Xu TT, Qiu YQ, Liu NY, Ke XY, Fang L, Yan JP, Zhu DY. Homocysteine induced a calcium-mediated disruption of mitochondrial function and dynamics in endothelial cells. J Biochem Mol Toxicol 2021;35(5):e22737. https://doi.org/10.1002/jbt.22737.

Chester K, et al. Bioautography-based Identification of Antioxidant Metabolites of Solanum nigrum L. and Exploration Its Hepatoprotective Potential. Pharmacogn Mag 2017;13 (Suppl(62):179–88. https://doi.org/10.4103/pm.pm.

Claiborne A. Catalase activity. In: Greenwald RA, editor. CRC Handbook of Methods for Oxygen Radical Research. Boca Raton: CRC Press; 1985. p. 283–4.

Coore HG, Denton RM, Martin BR, Randle PJ. Regulation of adipose tissue pyruvate dehydrogenase by insulin and other hormones. Biochem J 1971;125:115–27.

Damian-Buda AC, Matei DM, Ciobanu L, Damian-Buda DZ, Pop RM, Buzoianu AD, Bocsan IC. Nesfatin-1: A Novel Diagnostic and Prognostic Biomarker in Digestive Diseases. Biomedicines 2024;12(8):1913. https://doi.org/10.3390/biomedicines12081913.

Dong J, Xu H, Xu H, Wang PF, Cai GJ, Song HF, Wang CC, Dong ZT, Ju YJ, Jiang ZY. Nesfatin-1 stimulates fatty-acid oxidation by activating AMP-activated protein kinase in STZ-induced type 2 diabetic mice. PLoS One 2013;8(12):e83397. https://doi.org/10.1371/journal.pone.0083397.

Dore R, Krotenko R, Reising JP, Murru L, Sundaram SM, Di Spiezio A, Müller-Fielitz H, Schwaninger M, Jöhren O, Mittag J, Passafaro M, Shanabrough M, Horvath TL, Schulz C, Lehnert H. Nesfatin-1 decreases the motivational and rewarding value of food. Neuropsychopharmacology 2020;45(10):1645–55. https://doi.org/10.1038/s41386-020-0682-3.

Ellman GL. Tissue sulfhydryl groups. Arch Biochem Biophys 1959;82:70–7.

Ellman GL, Courtney KD, Andres V Jr, Feather-Stone RM. A new and rapid colorimetric determination of acetylcholinesterase activity. Biochem Pharmacol 1961;7:88–95.

Ennaceur A, Delacour J. A new one-trial test for neurobiological studies of memory in rats. 1: Behavioral data. Behav Brain Res 1988;31:47–59.

Fan Z, Dong J, Mu Y, Liu X. Nesfatin-1 protects against diabetic cardiomyopathy in the streptozotocin-induced diabetic mouse model via the p38-MAPK pathway. Bioengineered 2022;13(6):14670–81.

Fiske CH, Subbarow Y. The colorimetric determination of phosphorus. J Biol Chem 1925;66:375–400.

Goebel M, Stengel A, Wang L, Taché Y. Central nesfatin-1 reduces the nocturnal food intake in mice by reducing meal size and increasing inter-meal intervals. Peptides 2011;32(1):36–43. https://doi.org/10.1016/j.peptides.2010.09.027.

Goebel-Stengel M, Stengel A. Role of brain NUCB2/nesfatin-1 in the stress-induced modulation of gastrointestinal functions. Curr Neuropharmacol 2016;14(8):882–91.

Gorelick PB, Counts SE, Nyenhuis D. Vascular cognitive impairment and dementia. Biochim Biophys Acta 2016;1862(5):860–8. https://doi.org/10.1016/j.bbadis.2015.12.015.

Griffiths DE, Houghton RL. Studies on energy linked reactions: modified mitochondrial ATPase of oligomycin-resistant mutants of Saccharomyces cerevisiae. Eur J Biochem 1974;46:157–67.

Grisham MB, Benoit JN, Granger DN. Assessment of leukocyte involvement during ischemia and reperfusion of intestine. Methods Enzymol 1990;186:729–42. https://doi.org/10.1016/0076-6879(90)86172-r.

He Y, He T, Li H, Chen W, Zhong B, Wu Y, Chen R, Hu Y, Ma H, Wu B, Hu W, Han Z. Deciphering

mitochondrial dysfunction: Pathophysiological mechanisms in vascular cognitive impairment. Biomed Pharmacother 2024;174:116428. https://doi.org/10.1016/j.biopha.2024.116428.

Hemanth Kumar B, Dinesh Kumar B, Diwan PV. Hesperidin, a citrus flavonoid, protects against l-methionine-induced hyperhomocysteinemia by abrogation of oxidative stress, endothelial dysfunction and neurotoxicity in Wistar rats. Pharm Biol 2017;55(1):146–55. https://doi.org/10.1080/13880209.2016.1231695.

Hissin PJ, Hilf R. A fluorometric method for determination of oxidized and reduced glutathione in tissues. Anal Biochem 1976;74:214–26.

Huang Y, Wu H, Hu Y, Zhou C, Wu J, Wu Y, Wang H, Lenahan C, Huang L, Nie S, Gao X, Sun J. Puerarin Attenuates Oxidative Stress and Ferroptosis via AMPK/PGC1α/Nrf2 Pathway after Subarachnoid Hemorrhage in Rats. Antioxidants 2022;11(7):1259. https://doi.org/10.3390/antiox11071259.

Jiménez-Ruiz A, Aguilar-Fuentes V, Becerra-Aguiar NN, Roque-Sanchez I, Ruiz-Sandoval JL. Vascular cognitive impairment and dementia: a narrative review. Dement Neuropsychol 2024;18:e20230116. https://doi.org/10.1590/1980-5764-DN-2023-0116.

Kamboj SS, Kumar V, Kamboj A, Sandhir R. Mitochondrial oxidative stress and dysfunction in rat brain induced by carbofuran exposure. Cell Mol Neurobiol 2008;28(7):961–9. https://doi.org/10.1007/s10571-008-9270-5.

Kaplan P, Tatarkova Z, Sivonova MK, Racay P, Lehotsky J. Homocysteine and Mitochondria in Cardiovascular and Cerebrovascular Systems. Int J Mol Sci 2020;21(20):7698. https://doi.org/10.3390/ijms21207698.

Khan FH, Sen T, Maiti AK, Jana S, Chatterjee U, Chakrabarti S. Inhibition of rat brain mitochondrial electron transport chain activity by dopamine oxidation products during extended in vitro incubation: implications for Parkinson's disease. Biochim Biophys Acta 2005;1741(1-2):65–74. https://doi.org/10.1016/j.bbadis.2005.03.013.

Khan MB, Hafez S, Hoda MN, Baban B, Wagner J, Awad ME, Sangabathula H, Haigh S, Elsalanty M, Waller JL, Hess DC. Chronic remote ischemic conditioning is cerebroprotective and induces vascular remodeling in a VCID model. Transl Stroke Res 2018;9(1):51–63.

Khodir SA, Faried MA, Abd-Elhafiz HI, Sweed EM. Sitagliptin Attenuates the Cognitive Deficits in L-Methionine-Induced Vascular Dementia in Rats. BioMed Res Int 2022;2022:7222590. https://doi.org/10.1155/2022/7222590.

King TE, Howard RL. Preparation and properties of soluble NADH dehydrogenase from cardiac muscle. Methods Enzymol 1967;10:322–31.

King TE, Ohnishi T, Winter DB, Wu JT. Biochemical and EPR probes for structure–function studies of iron sulfur centers of succinate dehydrogenase. Adv Exp Med Biol 1976;74:182–227.

Kumar M, Bansal N. Fasudil hydrochloride ameliorates memory deficits in rat model of streptozotocin-induced Alzheimer's disease: Involvement of PI3-kinase, eNOS and NFκB. Behav Brain Res 2018a;351:4–16. https://doi.org/10.1016/j.bbr.2018.05.024.

Kumar M, Bansal N. Fasudil hydrochloride ameliorates memory deficits in rat model of streptozotocin-induced Alzheimer's disease: Involvement of PI3-kinase, eNOS and NFκB. Behav Brain Res 2018b;351:4–16.

Kumar M, Sandhir R. Hydrogen sulfide attenuates hyperhomocysteinemia-induced mitochondrial dysfunctions in brain. Mitochondrion 2020;50:158–69. https://doi.org/10.1016/j.mito.2019.11.004.

Kumar M, Singh G, Kushwah AS, Surampalli G, Singh TG, Gupta S. Arbutin protects brain against middle cerebral artery occlusion-reperfusion (MCAo/R) injury. Biochem Biophys Res Commun 2021;577:52–7. https://doi.org/10.1016/j.bbrc.2021.09.006.

Liu KZ, Schultz CP, Johnston JB, Lee K, Mantsch HH. Comparison of infrared spectra of CLL cells with their ex vivo sensitivity (MTT assay) to chlorambucil and cladribine. Leuk Res 1997;21:1125–33.

Liu Y, et al. Central nesfatin-1 activates lipid mobilization in adipose tissue and fatty acid oxidation in muscle via the sympathetic nervous system. BioFactors 2020;46(3):454–64. https://doi.org/10.1002/biof.1600.

Lowry OH, Rosebrough NJ, Farr AL, Randall RJ. Protein measurement with the Folin phenol reagent. J Biol Chem 1951;193(1):265–75.

Mangat GS, Jaggi AS, Singh N. Ameliorative Effect of a Selective Endothelin ETA Receptor Antagonist in Rat Model of L-Methionine-induced Vascular Dementia. Korean J Physiol Pharmacol 2014;18(3):201–9.

Moosavi M, Abbasi L, Zarifkar A, Rastegar K. The role of nitric oxide in spatial memory stages, hippocampal ERK and CaMKII phosphorylation. Pharmacol Biochem Behav 2014;122:164–72.

Morris RGM. Development of a water-maze procedure for studying spatial learning in the rats. J Neurosci Methods 1984;11:47–60.

Mortazavi S, Gonzalez R, Ceddia R, Unniappan S. Long-term infusion of nesfatin-1 causes a sustained regulation of whole-body energy homeostasis of male Fischer 344 rats. Front Cell Dev Biol 2015;3:22. https://doi.org/10.3389/fcell.2015.00022.

Ohkawa H, Ohishi N, Yagi K. Assay for lipid peroxides in animal tissues by thiobarbituric acid reaction. Anal Biochem 1979;95:351–8.

Oyamada N, Sone M, Miyashita K, Park K, Taura D, Inuzuka M, Sonoyama T, Fukunaga Y, Tamura N, Itoh H, Nakao K. The role of mineralocorticoid receptor expression in brain remodeling after cerebral ischemia. Endocrinology 2008;149(8):3764–77.

Patai R, Patel K, Csik B, Gulej R, Nagaraja RY, Nagy D, Chandragiri SS, Shanmugarama S, Kordestan KV, Nagykaldi M, Ekambaram S, Ungvari A, Yabluchanskiy A, Tarantini S, Benyo Z, Csiszar A, Ungvari Z, Nyul-Toth A. Aging, mitochondrial dysfunction, and cerebral microhemorrhages: a preclinical evaluation of SS-31 (elamipretide) and development of a high-throughput machine learning-driven imaging pipeline for cerebromicrovascular protection therapeutic screening. Geroscience 2025;47(3):4871–87. https://doi.org/10.1007/s11357-025-01634-5.

Paxinos G, Watson C. The rat brain in stereotaxic coordinates. 2nd ed. Sydney: Academic Press; 1986.

Perez-Pinzon MA, Xu GP, Born J, Lorenzo J, Busto R, Rosenthal M, Sick TJ. Cytochrome C is released from mitochondria into the cytosol after cerebral anoxia or ischemia. J Cereb Blood Flow Metab 1999;19:39–46.

Postnikova TY, Griflyuk AV, Tumanova NL, Dubrovskaya NM, Mikhel AV, Vasilev DS, Zaitsev AV. Prenatal Hyperhomocysteinemia Leads to Synaptic Dysfunction and Structural Alterations in the CA1 Hippocampus of Rats. Biomolecules 2025;15(2):305.

Puka-Sundvall M, Eriksson P, Nilsson M, Sandberg M, Lehmann A. Neurotoxicity of cysteine: interaction with glutamate. Brain Res 1995;705:65–70.

Reddy DS, Kulkarni SK. Possible role of nitric oxide in the nootropic and antiamnesic effects of neurosteroids on aging- and dizocilpine-induced learning impairment. Brain Res 1998;799(2):215–29. https://doi.org/10.1016/S0006-8993(98)00419-3.

Reznick AZ, Packer L. Oxidative damage to proteins: Spectrophotometric method for carbonyl assay. Methods Enzymol 1994;233:357–63. https://doi.org/10.1016/s0076-6879(94)33041-7.

Sandhir R, Sood A, Mehrotra A, Kamboj SS. N-Acetylcysteine reverses mitochondrial dysfunctions and behavioral abnormalities in 3-nitropropionic acid-induced Huntington's disease. Neurodegener Dis 2012;9(3):145–57. https://doi.org/10.1159/000334273.

Sastry KV, Moudgal RP, Mohan J, Tyagi JS, Rao GS. Spectrophotometric determination of serum nitrite and nitrate by copper-cadmium alloy. Anal Biochem 2002;306(1):79–82.

Saxena G, Bharti S, Kamat PK, Sharma S, Nath C. Melatonin alleviates memory deficits and neuronal degeneration induced by intracerebroventricular administration of streptozotocin in rats. Pharmacol Biochem Behav 2010;94(3):397–403. https://doi.org/10.1016/j.pbb.2009.09.022.

Schalla MA, Stengel A. Current Understanding of the Role of Nesfatin-1. J Endocr Soc 2018;2(10):1188–206. https://doi.org/10.1210/js.2018-00246.

Shah DI, Singh M. Inhibition of protein tyrosin phosphatase improves vascular endothelial dysfunction. Vascul Pharmacol 2006;44(3):177–82.

Shimizu H, Oh-I S, Hashimoto K, Nakata M, Yamamoto S, Yoshida N, Eguchi H, Kato I, Inoue K, Satoh T, Okada S, Yamada M, Yada T, Mori M. Peripheral administration of nesfatin-1 reduces food intake in mice: the leptin-independent mechanism. Endocrinology 2009;150(2):662–71. https://doi.org/10.1210/en.2008-0598.

Shimizu S, Narita M, Tsujimoto Y. Bcl-2 family proteins regulate the release of apoptogenic cytochrome c by the mitochondrial channel VDAC. Nature 1999;399:483–7.

Silva NCBS, Bracko O, Nelson AR, de Oliveira FF, Robison LS, Shaaban CE, Hainsworth AH, Price BR. Vascular cognitive impairment and dementia: An early career researcher perspective. Alzheimers Dement 2022;14(1):e12310. https://doi.org/10.1002/dad2.12310.

Škovierová H, Vidomanová E, Mahmood S, Sopková J, Drgová A, Červeňová T, Halašová E, Lehotský J. The Molecular and Cellular Effect of Homocysteine Metabolism Imbalance on Human Health. Int J Mol Sci 2016;17(10):1733. https://doi.org/10.3390/ijms17101733.

Smith EE, Aparicio HJ, Gottesman RF, Goyal MS, Greenberg SM, Schneider JA, Sorond FA, Wright CB, American Heart Association Stroke Council; Council on Cardiovascular and Stroke Nursing; and Council on Peripheral Vascular Disease. Vascular Contributions to Cognitive Impairment and Dementia in the United States: Prevalence and Incidence: A Scientific Statement From the American Heart Association. Stroke 2025;56(10):e317–30. https://doi.org/10.1161/STR.0000000000000494.

Solmaz A, Bahadır E, Gülçiçek OB, Yiğitbaş H, Çelik A, Karagöz A, Özsavcı D, Şirvancı S, Yeğen BÇ. Nesfatin-1 improves oxidative skin injury in normoglycemic or hyperglycemic rats. Peptides 2016;78:1–10.

Sottocasa GL, Kuylenstierna B, Ernster L, Bergstrand A. An electron transport system associated with the outer membrane of liver mitochondria, a biochemical and morphological study. J Cell Biol 1967;32:415–38.

Suryavanshi PS, Ugale RR, Yilmazer-Hanke D, Stairs DJ, Dravid SM. GluN2C/GluN2D subunit-selective NMDA receptor potentiator CIQ reverses MK-801-induced impairment in prepulse inhibition and working memory in Y-maze test in mice. Br J Pharmacol 2014;171(3):799–809. https://doi.org/10.1111/bph.12518.

Suzuki K. Measurement of Mn-SOD and Cu, Zn-SOD. In: Taniguchi N, Gutteridge MCJ, editors. Experimental Protocols for Reactive Oxygen and Nitrogen Species. Oxford, NY: Oxford University Press; 2000. p. 91–5.

Tan Z, Xu H, Shen X, Jiang H. Nesfatin-1 antagonized rotenone-induced neurotoxicity in MES23.5 dopaminergic cells. Peptides 2015;69:109–14. https://doi.org/10.1016/j.peptides.2015.04.019.

Tedeshi H, Harris DL. Some observations on the photometric estimation of mitochondrial volume. Biochim Biophys Acta 1958;28:392–402.

Varbiro G, Veres B, Gallyas F Jr, Sumegi B. Direct effect of taxol on free radical formation and mitochondrial permeability transition. Free Radic Biol Med 2001;31:548–58.

Victor T, Jordann AM, Bester AJ, Lochner A. A sensitive and rapid method for separating adenine nucleotides and creatine phosphate by ion-pair reversed-phase high-performance liquid chromatography. J Chromatogr 1987;389:339–44.

Vorhees CV, Williams MT. Morris water maze: procedures for assessing spatial and related forms of

learning and memory. Nat Protoc 2006;1(2):848–58. https://doi.org/10.1038/nprot.2006.116.

Wang P, Wang Y, Zhang Q, Zhang H, Li Z, Liu X, Kaur L, Kumar M. Amelioration of cognitive deficits by Spirulina platensis in L-methionine-induced rat model of vascular dementia. Pharmacogn Mag 2020;16:133–41.

Xu Y, Chen F. Antioxidant, anti-inflammatory and anti-apoptotic activities of nesfatin-1: a review. J Inflamm Res 2020;13:607–17.

Xu Y, Kabba JA, Ruan W, Wang Y, Zhao S, Song X, Zhang L, Li J, Pang T. The PGC-1α Activator ZLN005 Ameliorates Ischemia-Induced Neuronal Injury In Vitro and In Vivo. Cell Mol Neurobiol 2018;38(4):929–39. https://doi.org/10.1007/s10571-017-0567-0.

Yan LJ, Traber MG, Packer L. Spectrophotometric method for determination of carbonyls in oxidatively modified apolipoprotein B of human low-density lipoproteins. Anal Biochem 1995;228:349–51. https://doi.org/10.1006/abio.1995.1362.

Yin Y, Li Z, Gao L, Li Y, Zhao J, Zhang W. AMPK-dependent modulation of hepatic lipid metabolism by nesfatin-1. Mol Cell Endocrinol 2015;417:20–6.

Yu H, Liu Q, Xie M, Fan J, Luo J, Huang J, Chen L. Nesfatin-1 inhibits cerebral aneurysms by activating Nrf2 and inhibiting NF-κB signaling. CNS Neurosci Ther 2024;30(8):e14864.

Zaborszky L, Wouterlood FG, Lanciego JL, editors. Neuroanatomical Tract-Tracing 3: Molecules, Neurons, and Systems. Springer; 2006. p. 372.

Zarrin A, Roshankar-Roodsari S, Zarei H, Dizaji SR, Ahmadzadeh K, Miri R, Yousefifard M. The therapeutic effect of Nesfatin-1 on acute myocardial ischemia/reperfusion injury; a systematic review and meta-analysis. Iran J Emerg Med 2023;10(1):e7.

Zhang T, Huang D, Hou J, Li J, Zhang Y, Tian M, Li Z, Tie T, Cheng Y, Su X, Man Z, Ma Y. High-concentration homocysteine inhibits mitochondrial respiration function and production of reactive oxygen species in neuron cells. J Stroke Cerebrovasc Dis 2020;29(10):105109. https://doi.org/10.1016/j.jstrokecerebrovasdis.2020.105109.

Zhao LP, You T, Chan SP, Chen JC, Xu WT. Adropin is associated with hyperhomocysteine and coronary atherosclerosis. Exp Ther Med 2015;11(3):1065–70.

Zhao LP, You T, Chan SP, Chen JC, Xu WT. Adropin is associated with hyperhomocysteine and coronary atherosclerosis. Exp Ther Med 2016;11:1065–70.

Zhou S, Nao J. Nesfatin-1: A biomarker and potential therapeutic target in neurological disorders. Neurochem Res 2024a;49(1):38–51.

Zhou S, Nao J. Nesfatin-1: A Biomarker and Potential Therapeutic Target in Neurological Disorders. Neurochem Res 2024b;49(1):38–51. https://doi.org/10.1007/s11064-023-04037-0.